Journal of Solid Mechanics Vol. 16, No. 3 (2024) pp. 246-267
DOI: 10.60664/jsm.2024.1130439

Research Paper

A New 3D Elasticity Numerical Solution For Nonlinear Thermo-Mechanical Bending of Orthotropic Annular/Circular Micro/Nano Plates Using Re-Modified Couple Stress & SAPM

A.R. Golkarian [1], M. Jabbarzadeh [2*]

[1] *Ph.D. Student, Science & Research Branch, Islamic Azad University, Tehran, Iran*
[2] *Department of Mechanical Engineering, Mashhad Branch, Islamic Azad University, Mashhad, Iran*

Received 29 August 2024; Received in revised form 25 September 2024; Accepted 3 October 2024

ABSTRACT

In this research, a new 3D elasticity numerical solution based on the Semi-Analytical Polynomial Method (SAPM) is presented for the nonlinear bending analysis of orthotropic annular/circular micro/nano plates resting on a Winkler-Pasternak elastic foundation, utilizing re-modified couple stress theory. This is the first report of a 3D elasticity numerical solution specifically based on re-modified couple stress theory. Moreover, while previous 3D analytical solutions based on couple stress theory have primarily focused on the bending of rectangular plates with simply supported edges, this study investigates the nonlinear bending of circular plates under various boundary conditions. Additionally, the variation in thickness under different types of loading (mechanical, thermal, and thermo-mechanical) is reported for the first time. The effects of boundary conditions, couple stress scale parameters, aspect ratio, thickness, loading, and the elastic foundation are examined. Both the increasing and decreasing impacts of scale parameters on deflection are observed in this study.

Keywords: Three dimensional elasticity theory; Re-modified couple stress theory; Semi-analytical polynomial method; Annular nanoplate; Nonlinear bending; Orthotropic material.

[*]Corresponding author. Tel. / Fax: +98 5136625046.
E-mail address: jabbarzadeh@mshdiau.ac.ir (M. Jabbarzadeh)

.

JOURNAL OF SOLID MECHANICS JSM

1 INTRODUCTION

NANOTECHNOLOGY is one of the most intriguing research fields across various branches of science. The unique properties of nanomaterials and the challenges posed by experimental studies at the nanoscale motivate researchers to explore their mechanical properties through various theoretical or semi-experimental methods. As a result, theoretical approaches such as the Molecular Mechanics Method (MMM) [1-5] and the Molecular Dynamics Method (MDM) [6,7] have been introduced and employed to investigate these properties, both of which are grounded in molecular and mechanical sciences. Among the mechanical properties, only stretching properties and vibration frequencies can be experimentally evaluated due to the limitations of available instruments. Other mechanical properties, such as buckling behavior, must be assessed using MMM and MDM. However, certain analyses, such as bending, cannot be evaluated experimentally or even through molecular-based methods. Due to these limitations, alternative theoretical mechanical approaches, such as mechanical plate theories, are employed to examine the bending behavior of micro or nanoplates, some of which are mentioned here.

Experimental observations reveal that at the nanoscale, the mechanical behavior of structures is size-dependent. Since classical continuum theory neglects this size dependency, several non-classical continuum theories have been developed. These include classical couple stress theory [8–11], strain gradient theory [12], nonlocal elasticity [13], surface elasticity [14], and modified couple stress theory (MCST) [15]. Reddy and Berry [16] proposed nonlinear size-dependent models based on Classical Laminate Plate Theory (CLPT) and First-Order Shear Deformation Theory (FSDT) for the bending of circular plates. Reddy and Kim [17] utilized MCST and the nonlinear strains of von Karman to develop a size-dependent third-order plate model. Dastjerdi and Jabbarzadeh [18-23] employed Eringen's nonlocal theory and the Differential Quadrature Method (DQM), as well as introduced a new Semi-Analytical Polynomial Method (SAPM), to investigate the nonlinear thermo-mechanical bending of monolayer and bilayer graphene sheets based on FSDT and Third-Order Shear Deformation Theory (TSDT).Thai et al. [24–26] proposed new models based on Classical Plate Theory (CPT), FSDT, TSDT, and sinusoidal shear deformation plate theories for analyzing the bending and free vibration of rectangular microplates with simply-supported edges. Sahmani and Ansari [27] analyzed the free vibration of rectangular microplates using strain gradient theory and TSDT. Using nonlocal elasticity and a Higher-Order Shear Deformation Plate Theory (HSDT), Daneshmehr et al. [28] examined the size-dependent instability of nanoplates under biaxial in-plane loadings, solving the governing equations with the Generalized Differential Quadrature (GDQ) method. Also, there are some other valuable researches [29-35] which have examined nanomaterials from various aspects.

To the best of the authors' knowledge, no numerical study has been conducted on the bending analysis of circular plates (whether at the macro, micro, or nanoscale) based on 3D elasticity theory. In a few studies that utilize 3D analytical solutions, the bending of homogeneous or functionally graded (FG) rectangular plates subjected to sinusoidal transverse loading with simply supported edges has been examined [36-40]. Among these, the only research based on re-modified couple stress theory is the recent work by Salehipour et al. [40], which was the first to report a 3D analytical solution for the bending of FG micro/nanoplates. Additionally, the first report of finite element (FE) bending analysis of circular plates based on modified couple stress theory is by Reddy et al. [41], which is grounded in Classical Plate Theory (CPT) and First-Order Shear Deformation Theory (FSDT).

The absence of a numerical solution for 3D bending analysis in the literature is due to the challenges associated with developing such a solution for plates. Additionally, in existing analytical solutions, various restrictions on plate geometry (rectangular or circular), loading types, and boundary conditions are imposed to facilitate the solvability of the resulting governing equations. This study addresses this gap by introducing a new numerical approach to 3D elasticity solutions using the Semi-Analytical Polynomial Method (SAPM) recently presented by Dastjerdi and Jabbarzadeh [19]. For the first time, a novel numerical solution approach based on 3D elasticity theory is introduced for the nonlinear bending of annular/circular plates without imposing any restrictions on plate geometry or loading types, applicable to all boundary conditions.

This is also the first report of a 3D elasticity solution for the nonlinear bending analysis of orthotropic annular/circular micro/nanoplates based on re-modified couple stress theory. The analysis covers all boundary conditions, including clamped, simply supported, and free edges, under various types of loading such as mechanical, thermal, and thermo-mechanical. The effects of different elastic foundations, including Winkler, Pasternak, and Winkler-Pasternak, are also examined. Additionally, the influence of various parameters, particularly thermal loading, on the thickness variation of plates is investigated. The study explores the impact of all factors affecting plate deflection, including boundary conditions, couple stress scale parameters, aspect ratio, thickness, loading types, and elastic foundations.

2. GOVERNIN EQUATIONS

2.1 Re-modified couple stress theory

According to the Modified Couple Stress Theory (MCST) proposed by Yang et al. [42], the strain energy for an elastic and isotropic material within region V is [42]:

$$U = \frac{1}{2}\int_v (\sigma_{ij}:\varepsilon_{ij} + m_{ij}:\chi_{ij})dv \tag{1}$$

where $i, j = 1,2,3$ and σ_{ij} is the Cauchy stress tensor, ε_{ij} is the strain tensor, m_{ij} is the deviatory part of couple stress tensor and χ_{ij} is the symmetric curvature tensor which are defined respectively as [42]:

$$\sigma_{ij} = 2G\varepsilon_{ij} + \lambda\varepsilon_{kk}\delta_{ij} \tag{2}$$

$$\varepsilon_{ij} = \frac{1}{2}(u_{i,j} + u_{j,i} + u_{k,i}u_{k,j}) - \varepsilon_T\delta_{ij} \tag{3}$$

$$m_{ij} = 2l^2 G\chi_{ij} \tag{4}$$

$$\chi_{ij} = \frac{1}{2}(\omega_{i,j} + \omega_{j,i}) \tag{5}$$

where G and λ are Lame constants, u_i is the displacement vector, ε_{ij} is the stress tensor, l is the material length scale parameters (MLSP), ω_i is the rotation vector and δ_{ij} is Kronecker delta symbol which ε_T and ω_i are defined as [42]:

$$\varepsilon_T = \alpha\Delta T \tag{6}$$

$$\omega_i = \frac{1}{2}Curl(\vec{u}) \tag{7}$$

where α is thermal diffusivity and ΔT is the temperature difference.

Chen et al. [36] developed a re-modified couple stress theory for anisotropic elasticity, in which the curvature and couple stress tensors are redefined as [36]:

$$m_{ij} = l_i^2 G_i\chi_{ij} + l_j^2 G_j\chi_{ij} \tag{8}$$

$$\chi_{ij} = \omega_{i,j} \tag{9}$$

where l_i and G_i $(i = 1,2,3)$ are MLSPs and shear modules in different directions respectively.

2.2 3D elasticity theory formulation

A schematic of an annular/circular micro/nanoplate is shown in Fig.1 with an inner radius r_i, an outer radius r_o, and a thickness h subjected to uniform transverse loading q while resting on a Winkler-Pasternak elastic foundation

characterized by two parameters. k_w and k_p are the Winkler and Pasternak stiffness coefficients of elastic foundation, respectively. According to the 3D elasticity theory of plates, the displacements filed can be expressed as follow:

$$u_1(r,\theta,z) = u(r,\theta,z) \tag{10}$$

$$u_2(r,\theta,z) = v(r,\theta,z) \tag{11}$$

$$u_3(r,\theta,z) = w(r,\theta,z) \tag{12}$$

where u, v, w are the displacement components along the r,θ,z directions respectively and $v(r,\theta,z)$ is equal to zero due to the symmetry. It is obvious that no assumption or simplification is employed in definition of displacement vectors. Substituting Eqs. (10)-(12) into Eq. (3),the non-zero components of the Von-Karman strain field can be written as [41]:

$$\varepsilon_{rr} = \frac{\partial u}{\partial r} + \frac{1}{2}\left(\frac{\partial w}{\partial r}\right)^2 - \alpha\Delta\mathrm{T} \tag{13}$$

$$\varepsilon_{\theta\theta} = \frac{u}{r} - \alpha\Delta\mathrm{T} \tag{14}$$

$$\varepsilon_{zz} = \frac{\partial w}{\partial z} + \frac{1}{2}\left(\frac{\partial w}{\partial z}\right)^2 - \alpha\Delta\mathrm{T} \tag{15}$$

$$\varepsilon_{rz} = \left(\frac{\partial u}{\partial z} + \frac{\partial w}{\partial r} + \frac{\partial w}{\partial r}\frac{\partial w}{\partial z}\right) \tag{16}$$

Due to the symmetry of the geometry and boundary conditions, other strain components are zero. Substituting Eqs. (10)–(12) into Eqs. (7) and (9) yields the non-zero components of curvature as [41]:

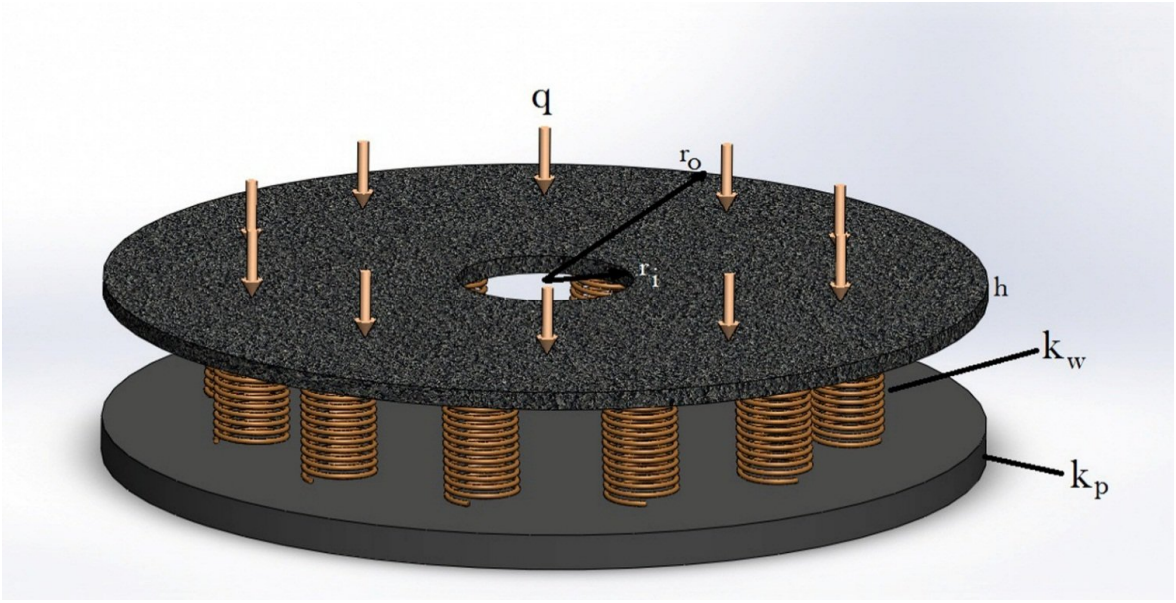

Fig. 1
The schematic view of an annular/circular graphitic plate under uniform loading and rested on elastic foundation.

$$\chi_{r\theta}=\frac{1}{4}\left(\frac{\partial^2 u}{\partial r\partial z}-\frac{\partial^2 w}{\partial r^2}\right) \tag{17}$$

$$\chi_{\theta r}=\frac{1}{4}\left(\frac{1}{r}\frac{\partial w}{\partial r}-\frac{1}{r}\frac{\partial u}{\partial z}\right) \tag{18}$$

$$\chi_{\theta z}=\frac{1}{4}\left(\frac{\partial^2 u}{\partial z^2}-\frac{\partial^2 w}{\partial z\partial r}\right) \tag{19}$$

Due to the orthotropic behavior of the employed micro/nanoplates, the stress-strain relations are derived as follows [43]:

$$\sigma_{rr}=\frac{E_r}{\kappa}\left[\left(1-\upsilon_{\theta z}\upsilon_{z\theta}\right)\varepsilon_{rr}+\left(\upsilon_{\theta r}+\upsilon_{\theta z}\upsilon_{zr}\right)\varepsilon_{\theta\theta}+\left(\upsilon_{zr}+\upsilon_{\theta r}\upsilon_{z\theta}\right)\varepsilon_{zz}-\left(\left(1-\upsilon_{\theta z}\upsilon_{z\theta}\right)\left(\upsilon_{\theta r}+\upsilon_{\theta z}\upsilon_{zr}\right)\left(\upsilon_{zr}+\upsilon_{\theta r}\upsilon_{z\theta}\right)\right)\alpha\Delta T\right] \tag{20}$$

$$\sigma_{\theta\theta}=\frac{E_r}{\kappa}\left[\left(\upsilon_{r\theta}+\upsilon_{rz}\upsilon_{z\theta}\right)\varepsilon_{rr}+\left(1-\upsilon_{rz}\upsilon_{zr}\right)\varepsilon_{\theta\theta}+\left(\upsilon_{z\theta}+\upsilon_{r\theta}\upsilon_{zr}\right)\varepsilon_{zz}-\left(\left(\upsilon_{r\theta}+\upsilon_{rz}\upsilon_{z\theta}\right)\left(1-\upsilon_{rz}\upsilon_{zr}\right)\left(\upsilon_{z\theta}+\upsilon_{r\theta}\upsilon_{zr}\right)\right)\alpha\Delta T\right] \tag{21}$$

$$\sigma_{zz}=\frac{E_r}{\kappa}\left[\left(\upsilon_{rz}+\upsilon_{r\theta}\upsilon_{\theta z}\right)\varepsilon_{rr}+\left(\upsilon_{\theta z}+\upsilon_{rz}\upsilon_{\theta r}\right)\varepsilon_{\theta\theta}+\left(1-\upsilon_{r\theta}\upsilon_{\theta r}\right)\varepsilon_{zz}-\left(\left(\upsilon_{rz}+\upsilon_{r\theta}\upsilon_{\theta z}\right)\left(\upsilon_{\theta z}+\upsilon_{rz}\upsilon_{\theta r}\right)\left(1-\upsilon_{r\theta}\upsilon_{\theta r}\right)\right)\alpha\Delta T\right] \tag{22}$$

$$\sigma_{rz}=G_{rz}\gamma_{rz} \tag{23}$$

where υ_{ij} is poison ratio, γ_{rz} is shear strain, E_r is the elastic module in r direction, G_{rz} is the shear module of orthotropic micro/nanoplate and $\kappa=1-\upsilon_{\theta z}\upsilon_{z\theta}-\upsilon_{r\theta}\upsilon_{\theta r}-\upsilon_{rz}\upsilon_{zr}-\upsilon_{r\theta}\upsilon_{\theta z}\upsilon_{zr}-\upsilon_{\theta r}\upsilon_{z\theta}\upsilon_{rz}$ which $\upsilon_{\theta r}=\upsilon_{r\theta}\times E_\theta/E_r$, $\upsilon_{zr}=\upsilon_{rz}\times E_z/E_r$ and $\upsilon_{z\theta}=\upsilon_{\theta z}\times E_z/E_\theta$. The E_θ and E_z are the elastic module in θ and z directions.

2.3 Constitutive equations

In this study, the constitutive equations and boundary conditions are derived based on the principle of minimum total potential energy, as follows [43]:

$$\delta\left(U-W_{ext}\right)=0 \tag{24}$$

where δ represents the variation symbol, and W_{ext} is the potential of applied forces, which includes the effects of transverse loading q and the Winkler-Pasternak elastic foundation on the surface of the micro/nanoplate. The components of the total potential energy are defined as follows:

$$\delta U=\left(\iint_A \sigma_{rr}\delta\varepsilon_{rr}+\sigma_{\theta\theta}\delta\varepsilon_{\theta\theta}+\sigma_{zz}\delta\varepsilon_{zz}+\sigma_{rz}\delta\gamma_{rz}+m_{r\theta}\delta\chi_{r\theta}+m_{\theta r}\delta\chi_{\theta r}+m_{\theta z}\delta\chi_{\theta z}\right)rdrdz \tag{25}$$

$$\delta W_{ext}=\int_{r_i}^{r_o}\left(q-k_w w+k_p\nabla^2 w\right)\delta w r dr \tag{26}$$

where $\nabla^2 = \frac{\partial^2}{\partial r^2} + \frac{1}{r}\frac{\partial}{\partial r}$ is the Laplacian operator.

The constitutive relations for orthotropic elasticity can be expressed as:

$$\sigma_{ij} = C\varepsilon_{ij} - D\varepsilon_T \tag{27}$$

where $\sigma_{ij} = [\sigma_{rr}\sigma_{\theta\theta}\sigma_{zz}\tau_{rz}m_{r\theta}m_{\theta r}m_{z\theta}m_{\theta z}]^T$, $\varepsilon_{ij} = [\varepsilon_{rr}\varepsilon_{\theta\theta}\varepsilon_{zz}\gamma_{rz}\chi_{r\theta}\chi_{\theta r}\chi_{z\theta}\chi_{\theta z}]^T$ and C is the stiffness matrix which based on re-modified coupled stress theory is defined as:

$$C = \begin{pmatrix} E_r(1-\upsilon_{\theta z}\upsilon_{z\theta})/\kappa & E_r(\upsilon_{\theta r}+\upsilon_{\theta z}\upsilon_{zr})/\kappa & E_r(\upsilon_{zr}+\upsilon_{\theta r}\upsilon_{z\theta})/\kappa & & & & & \\ E_r(\upsilon_{r\theta}+\upsilon_{rz}\upsilon_{z\theta})/\kappa & E_r(1-\upsilon_{rz}\upsilon_{zr})/\kappa & E_r(\upsilon_{z\theta}+\upsilon_{r\theta}\upsilon_{zr})/\kappa & & & & & \\ E_r(\upsilon_{rz}+\upsilon_{r\theta}\upsilon_{\theta z})/\kappa & E_r(\upsilon_{\theta z}+\upsilon_{rz}\upsilon_{\theta r})/\kappa & E_r(1-\upsilon_{r\theta}\upsilon_{\theta r})/\kappa & & & & & \\ & & & G_{rz} & & & & \\ & & & & G_{rz}l_r^2 & G_{\theta z}l_\theta^2 & & \\ & & & & G_{rz}l_r^2 & G_{\theta z}l_\theta^2 & & \\ & & & & & & G_{r\theta}l_r^2 & G_{\theta z}l_\theta^2 \\ & & & & & & G_{r\theta}l_r^2 & G_{\theta z}l_\theta^2 \end{pmatrix} \tag{28}$$

and D is the coefficients matrix of thermal strains as:

$$D = \frac{E_r}{\kappa}\begin{pmatrix} (1-\upsilon_{\theta z}\upsilon_{z\theta})(\upsilon_{\theta r}+\upsilon_{\theta z}\upsilon_{zr})(\upsilon_{zr}+\upsilon_{\theta r}\upsilon_{z\theta}) \\ (\upsilon_{r\theta}+\upsilon_{rz}\upsilon_{z\theta})(1-\upsilon_{rz}\upsilon_{zr})(\upsilon_{z\theta}+\upsilon_{r\theta}\upsilon_{zr}) \\ (\upsilon_{rz}+\upsilon_{r\theta}\upsilon_{\theta z})(\upsilon_{\theta z}+\upsilon_{rz}\upsilon_{\theta r})(1-\upsilon_{r\theta}\upsilon_{\theta r}) \\ 0 \\ 0 \\ 0 \\ 0 \\ 0 \end{pmatrix} \tag{29}$$

By substituting Eqs. (13)–(19) into Eq. (25) and neglecting body forces and external couples, the 3D equilibrium equations for an orthotropic annular/circular micro/nanoplate based on the re-modified couple stress theory are derived as follows:

$$\delta u = 0 : \frac{\partial \sigma_{rr}}{\partial r} + \frac{\partial \sigma_{rz}}{\partial z} + \frac{\sigma_r - \sigma_\theta}{r} + \frac{1}{2r}\left(r\frac{\partial^2 m_{r\theta}}{\partial r \partial z} + \frac{\partial m_{r\theta}}{\partial z} + \frac{\partial m_{\theta r}}{\partial z} + \frac{\partial^2 m_{\theta z}}{\partial z^2}\right) = 0 \tag{30}$$

$$\begin{aligned} \delta w = 0 : & \frac{\partial \sigma_{rz}}{\partial r} + \frac{\sigma_{rz}}{r} + \frac{\partial \sigma_z}{\partial z} + \frac{1}{r}\frac{\partial}{\partial r}\left(r\sigma_r \frac{\partial w}{\partial r} + r\sigma_{rz}\frac{\partial w}{\partial z}\right) + \frac{1}{r}\frac{\partial}{\partial z}\left(r\sigma_{rz}\frac{\partial w}{\partial r} + r\sigma_z \frac{\partial w}{\partial z}\right) + \\ & \frac{1}{2r}\left(-r\frac{\partial^2 m_{r\theta}}{\partial r^2} - 2\frac{\partial m_{r\theta}}{\partial r} - \frac{\partial m_{\theta r}}{\partial r}\right) = 0 \end{aligned} \tag{31}$$

For sake of generality and convenience, the following non-dimensional parameters are introduced:

$$\begin{aligned} & r^* = \frac{r}{r_i}, z^* = \frac{z}{r_i}, u^* = \frac{u}{r_i}, w^* = \frac{w}{r_i}, l_r^* = \frac{l_r}{h}, l_\theta^* = \frac{l_\theta}{h}, q^* = \frac{q}{E_r}, G_{rz}{}^* = \frac{G_{rz}}{E_r}, G_{\theta z}{}^* = \frac{G_{\theta z}}{E_r}, G_{r\theta}{}^* = \frac{G_{r\theta}}{E_r}, \\ & k_w{}^* = \frac{k_w \cdot r_i}{E_r}, k_p{}^* = \frac{k_p}{E_r \cdot r_i}, \eta = \frac{h}{r_i} \end{aligned} \tag{32}$$

As the final step, by substituting Eqs. (13)–(16) into Eqs. (20)–(23) to express the stress components, and Eqs. (17)–(19) into Eq. (8) to define the couple stress components in terms of the displacement fields, the stress terms in Eqs. (30) and (31) are replaced. Using non-dimensional parameters, two equilibrium equations are derived as follows:

$$\delta u = 0 : \frac{1}{\kappa}\left[\left(1-\upsilon_{\theta z}\upsilon_{z\theta}\right)\frac{\partial}{\partial r^*}\left(\frac{\partial u^*}{\partial r^*}+\frac{1}{2}\left(\frac{\partial w^*}{\partial r^*}\right)^2\right)+\left(\upsilon_{\theta r}+\upsilon_{\theta z}\upsilon_{zr}\right)\frac{\partial}{\partial r^*}\left(\frac{u^*}{r^*}\right)+\right.$$

$$\left.\left(\upsilon_{zr}+\upsilon_{\theta r}\upsilon_{z\theta}\right)\frac{\partial}{\partial r^*}\left(\frac{\partial w^*}{\partial z^*}+\frac{1}{2}\left(\frac{\partial w^*}{\partial z^*}\right)^2\right)\right]+G_{rz}^*\frac{\partial}{\partial z^*}\left(\frac{\partial u^*}{\partial z^*}+\frac{\partial w^*}{\partial r^*}+\frac{\partial w^*}{\partial r^*}\frac{\partial w^*}{\partial z^*}\right)+$$

$$\frac{1}{\kappa\cdot r^*}\left(1-\upsilon_{\theta z}\upsilon_{z\theta}\right)\left(\frac{\partial u^*}{\partial r^*}+\frac{1}{2}\left(\frac{\partial w^*}{\partial r^*}\right)^2-\alpha\Delta T\right)+\frac{1}{\kappa\cdot r^*}\left(\upsilon_{\theta r}+\upsilon_{\theta z}\upsilon_{zr}\right)\left(\frac{u^*}{r^*}-\alpha\Delta T\right)+$$

$$\frac{1}{\kappa\cdot r^*}\left(\upsilon_{zr}+\upsilon_{\theta r}\upsilon_{z\theta}\right)\left(\frac{\partial w^*}{\partial z^*}+\frac{1}{2}\left(\frac{\partial w^*}{\partial z^*}\right)^2-\alpha\Delta T\right)-\frac{\left(\left(1-\upsilon_{\theta z}\upsilon_{z\theta}\right)\left(\upsilon_{\theta r}+\upsilon_{\theta z}\upsilon_{zr}\right)\left(\upsilon_{zr}+\upsilon_{\theta r}\upsilon_{z\theta}\right)\alpha\Delta T\right)}{\kappa\cdot r^*}-$$

$$\frac{1}{\kappa\cdot r^*}\left(\upsilon_{r\theta}+\upsilon_{rz}\upsilon_{z\theta}\right)\left(\frac{\partial u^*}{\partial r^*}+\frac{1}{2}\left(\frac{\partial w^*}{\partial r^*}\right)^2-\alpha\Delta T\right)-\frac{1}{\kappa\cdot r^*}\left(1-\upsilon_{rz}\upsilon_{zr}\right)\left(\frac{u^*}{r^*}-\alpha\Delta T\right)-$$

$$\frac{1}{\kappa\cdot r^*}\left(\upsilon_{z\theta}+\upsilon_{r\theta}\upsilon_{zr}\right)\left(\frac{\partial w^*}{\partial z^*}+\frac{1}{2}\left(\frac{\partial w^*}{\partial z^*}\right)^2-\alpha\Delta T\right)+\frac{\left(\left(\upsilon_{r\theta}+\upsilon_{rz}\upsilon_{z\theta}\right)\left(1-\upsilon_{rz}\upsilon_{zr}\right)\left(\upsilon_{z\theta}+\upsilon_{r\theta}\upsilon_{zr}\right)\alpha\Delta T\right)}{\kappa\cdot r^*}+$$

$$\frac{\eta^2 l_r^{*2}G_{rz}^*}{8}\frac{\partial^2}{\partial r^*\partial z^*}\left(\frac{\partial^2 u^*}{\partial r^*\partial z^*}-\frac{\partial^2 w^*}{\partial r^{*2}}\right)+\frac{\eta^2 l_\theta^{*2}G_{\theta z}^*}{8}\frac{\partial^2}{\partial r^*\partial z^*}\left(\frac{1}{r^*}\frac{\partial w^*}{\partial r^*}-\frac{1}{r^*}\frac{\partial u^*}{\partial z^*}\right)+$$

$$\frac{\eta^2 l_r^{*2}G_{rz}^*}{4r^*}\frac{\partial}{\partial z^*}\left(\frac{\partial^2 u^*}{\partial r^*\partial z^*}-\frac{\partial^2 w^*}{\partial r^{*2}}\right)+\frac{\eta^2 l_\theta^{*2}G_{\theta z}^*}{4r^*}\frac{\partial}{\partial z^*}\left(\frac{1}{r^*}\frac{\partial w^*}{\partial r^*}-\frac{1}{r^*}\frac{\partial u^*}{\partial z^*}\right)+\frac{\eta^2 l_\theta^{*2}G_{\theta z}^*}{8r^*}\frac{\partial^2}{\partial z^{*2}}\left(\frac{\partial^2 u^*}{\partial z^{*2}}-\frac{\partial^2 w^*}{\partial z^*\partial r^*}\right)=0 \quad (33)$$

$$\delta w = 0 : G_{rz}^{*}\frac{\partial}{\partial r^{*}}\left(\frac{\partial u^{*}}{\partial z^{*}}+\frac{\partial w^{*}}{\partial r^{*}}+\frac{\partial w^{*}}{\partial r^{*}}\frac{\partial w^{*}}{\partial z^{*}}\right)+\frac{G_{rz}^{*}}{r^{*}}\frac{\partial}{\partial r^{*}}\left(\frac{\partial u^{*}}{\partial z^{*}}+\frac{\partial w^{*}}{\partial r^{*}}+\frac{\partial w^{*}}{\partial r^{*}}\frac{\partial w^{*}}{\partial z^{*}}\right)+$$
$$\frac{1}{\kappa}\left(\upsilon_{rz}+\upsilon_{r\theta}\upsilon_{\theta z}\right)\frac{\partial}{\partial z^{*}}\left(\frac{\partial u^{*}}{\partial r^{*}}+\frac{1}{2}\left(\frac{\partial w^{*}}{\partial r^{*}}\right)^{2}\right)+\frac{1}{\kappa}\left(\upsilon_{\theta z}+\upsilon_{rz}\upsilon_{\theta r}\right)\frac{\partial}{\partial z^{*}}\left(\frac{u^{*}}{r^{*}}\right)+\frac{1}{\kappa}\left(1-\upsilon_{r\theta}\upsilon_{\theta r}\right)\frac{\partial}{\partial z^{*}}\left(\frac{\partial w^{*}}{\partial z^{*}}+\frac{1}{2}\left(\frac{\partial w^{*}}{\partial z^{*}}\right)^{2}\right)$$
$$+\frac{1}{\kappa}\left(1-\upsilon_{\theta z}\upsilon_{z\theta}\right)\frac{\partial}{\partial r^{*}}\left[\left(\frac{\partial u^{*}}{\partial r^{*}}+\frac{1}{2}\left(\frac{\partial w^{*}}{\partial r^{*}}\right)^{2}\right)\frac{\partial w^{*}}{\partial r^{*}}\right]+\frac{1}{\kappa}\left(\upsilon_{\theta r}+\upsilon_{\theta z}\upsilon_{zr}\right)\frac{\partial}{\partial r^{*}}\left[\left(\frac{u^{*}}{r^{*}}\right)\frac{\partial w^{*}}{\partial r^{*}}\right]+$$
$$\frac{1}{\kappa}\left(\upsilon_{zr}+\upsilon_{\theta r}\upsilon_{z\theta}\right)\frac{\partial}{\partial r^{*}}\left[\left(\frac{\partial w^{*}}{\partial z^{*}}+\frac{1}{2}\left(\frac{\partial w^{*}}{\partial z^{*}}\right)^{2}\right)\frac{\partial w^{*}}{\partial r^{*}}\right]-\frac{1}{\kappa}\frac{\partial}{\partial r^{*}}\left[\left(\left(1-\upsilon_{\theta z}\upsilon_{z\theta}\right)\left(\upsilon_{\theta r}+\upsilon_{\theta z}\upsilon_{zr}\right)\left(\upsilon_{zr}+\upsilon_{\theta r}\upsilon_{z\theta}\right)\alpha\Delta T\right)\frac{\partial w^{*}}{\partial r^{*}}\right]$$
$$+G_{rz}^{*}\frac{\partial}{\partial r^{*}}\left(\frac{\partial u^{*}}{\partial z^{*}}+\frac{\partial w^{*}}{\partial r^{*}}+\frac{\partial w^{*}}{\partial r^{*}}\frac{\partial w^{*}}{\partial z^{*}}\right)\frac{\partial w^{*}}{\partial z^{*}}+G_{rz}^{*}\frac{\partial}{\partial z^{*}}\left(\frac{\partial u^{*}}{\partial z^{*}}+\frac{\partial w^{*}}{\partial r^{*}}+\frac{\partial w^{*}}{\partial r^{*}}\frac{\partial w^{*}}{\partial z^{*}}\right)\frac{\partial w^{*}}{\partial r^{*}}+\frac{1}{\kappa}\left(\upsilon_{rz}+\upsilon_{r\theta}\upsilon_{\theta z}\right)\frac{\partial}{\partial z^{*}}$$
$$\left[\left(\frac{\partial u^{*}}{\partial r^{*}}+\frac{1}{2}\left(\frac{\partial w^{*}}{\partial r^{*}}\right)^{2}\right)\frac{\partial w^{*}}{\partial z^{*}}\right]+\frac{1}{\kappa}\left(\upsilon_{\theta z}+\upsilon_{rz}\upsilon_{\theta r}\right)\frac{\partial}{\partial z^{*}}\left[\left(\frac{u^{*}}{r^{*}}\right)\frac{\partial w^{*}}{\partial z^{*}}\right]+\frac{1}{\kappa}\left(1-\upsilon_{r\theta}\upsilon_{\theta r}\right)\frac{\partial}{\partial z^{*}}\left[\left(\frac{\partial w^{*}}{\partial z^{*}}+\frac{1}{2}\left(\frac{\partial w^{*}}{\partial z^{*}}\right)^{2}\right)\frac{\partial w^{*}}{\partial z^{*}}\right]$$
$$-\frac{1}{\kappa}\left(\upsilon_{rz}+\upsilon_{r\theta}\upsilon_{\theta z}\right)\left(\upsilon_{\theta z}+\upsilon_{rz}\upsilon_{\theta r}\right)\left(1-\upsilon_{r\theta}\upsilon_{\theta r}\right)\alpha\Delta T-\frac{\eta^{2}l_{r}^{*2}G_{rz}^{*}}{8}\frac{\partial^{2}}{\partial r^{*2}}\left(\frac{\partial^{2}u^{*}}{\partial r^{*}\partial z^{*}}-\frac{\partial^{2}w^{*}}{\partial r^{*2}}\right)-$$
$$\frac{\eta^{2}l_{\theta}^{*2}G_{\theta z}^{*}}{8}\frac{\partial^{2}}{\partial r^{*2}}\left(\frac{1}{r^{*}}\frac{\partial w^{*}}{\partial r^{*}}-\frac{1}{r^{*}}\frac{\partial u^{*}}{\partial z^{*}}\right)-\frac{3\eta^{2}l_{r}^{*2}G_{rz}^{*}}{8r^{*}}\frac{\partial}{\partial r^{*}}\left(\frac{\partial^{2}u^{*}}{\partial r^{*}\partial z^{*}}-\frac{\partial^{2}w^{*}}{\partial r^{*2}}\right)-$$
$$\frac{3\eta^{2}l_{\theta}^{*2}G_{\theta z}^{*}}{8r^{*}}\frac{\partial}{\partial r^{*}}\left(\frac{1}{r^{*}}\frac{\partial w^{*}}{\partial r^{*}}-\frac{1}{r^{*}}\frac{\partial u^{*}}{\partial z^{*}}\right)=0 \tag{34}$$

3. SOLUTION PROCEDURE

In this study, based on SAPM [20], by considering each partial differential equation (two equilibrium equations) as follows:

$$\frac{\partial^{n}F(r,z)}{\partial^{n}r}+\frac{\partial^{(n-1)}F(r,z)}{\partial^{(n-1)}r}+\cdots+\frac{\partial F(r,z)}{\partial r}+\frac{\partial^{n}F(r,z)}{\partial^{n}z}+\frac{\partial^{(n-1)}F(r,z)}{\partial^{(n-1)}z}+\cdots+$$
$$\frac{\partial F(r,z)}{\partial z}+\frac{\partial^{n}F(r,z)}{\partial r\partial^{(n-1)}z}+\frac{\partial^{n}F(r,z)}{\partial r^{2}\partial^{(n-2)}z}+\cdots+\frac{\partial^{n}F(r,z)}{\partial r^{(n-1)}\partial z}=0 \tag{35}$$

where the function $F(r,z)$ is defined as:

$$F(r,z)=\sum_{i=1}^{N}\sum_{j=1}^{M}a_{(i+j-(1-(i-1)(M-1)))}r^{(i-1)}z^{(j-1)} \tag{36}$$

where N is the number of grid points in r direction and M is the number of grid point in z direction, the partial differential equation is converted to the algebraic equation. The schematic view of grid points is illustrated in Fig. 2. The empty points must satisfy the equilibrium equations, while the filled points must satisfy the boundary conditions.

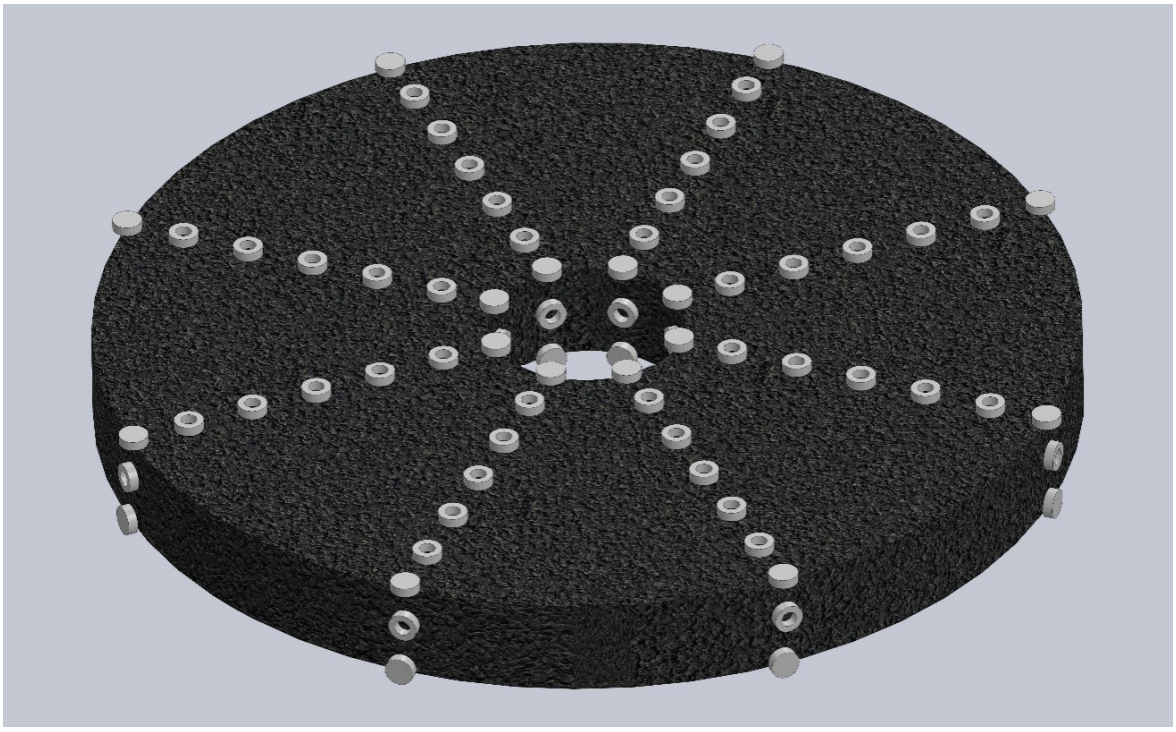

Fig. 2
The schematic view of grid points based on SAPM.

Based on the above explanations of SAPM, two displacement fields can be defined as follows:

$$u(r,z)=\sum_{i=1}^{N}\sum_{j=1}^{M}a_{(i+j-(1-(i-1)(M-1)))}r^{(i-1)}z^{(j-1)} \tag{37}$$

$$w(r,z)=\sum_{i=1}^{N}\sum_{j=1}^{M}a_{(i+j-(1-(i-1)(M-1))+M\cdot N)}r^{(i-1)}z^{(j-1)} \tag{38}$$

The obtained algebraic equations are solved using numerical methods, such as the Newton-Raphson method.

4. BOUNDARY CONDITIONS

In the present study, all types of boundary conditions are categorized into three types: simply supported (S), clamped (C), and free edges (F). At the inner and outer radii (ri and ro), the boundary conditions can be defined as follows:

$$S:\sigma_r=w^*=m_{r\theta}=m_{\theta z}=0 \tag{39}$$

$$C:u^*=w^*=\frac{\partial w^*}{\partial r^*}=\frac{\partial u^*}{\partial z^*}=0 \tag{40}$$

$$F:\sigma_r-\eta^2\frac{\partial m_{r\theta}}{\partial z^*}=\sigma_{rz}+\sigma_r\frac{\partial w^*}{\partial r^*}+\sigma_{rz}\frac{\partial w^*}{\partial z^*}+\eta^2\frac{\partial m_{r\theta}}{\partial r^*}+\eta^2\frac{m_{r\theta}+m_{\theta r}}{r^*}+\eta^2\frac{\partial m_{\theta z}}{\partial z^*}=m_{r\theta}=m_{\theta z}=0 \tag{41}$$

The displacement components should satisfy the following boundary conditions at the top and bottom surfaces of the plate:

$$\sigma_{rz}-\eta^2\frac{\partial m_{r\theta}}{\partial r^*}-\eta^2\frac{m_{r\theta}+m_{\theta r}}{r^*}-\eta^2\frac{\partial m_{\theta z}}{\partial z^*}\Big|_{z=-\frac{h}{2},\frac{h}{2}}=0 \tag{42}$$

$$\sigma_z+\sigma_z\frac{\partial w^*}{\partial z^*}+\sigma_{rz}\frac{\partial w^*}{\partial r^*}+\eta^2\frac{\partial m_{\theta z}}{\partial r^*}+\eta^2\frac{m_{\theta z}}{r^*}-q^*\Big|_{z=-\frac{h}{2}}=0 \tag{43}$$

$$m_{\theta z}\big|_{z=-\frac{h}{2},\frac{h}{2}}=m_{r\theta}\big|_{z=-\frac{h}{2},\frac{h}{2}}=0 \tag{44}$$

$$\sigma_z+\sigma_z\frac{\partial w^*}{\partial z^*}+\sigma_{rz}\frac{\partial w^*}{\partial r^*}+\eta^2\frac{\partial m_{\theta z}}{\partial r^*}+\eta^2\frac{m_{\theta z}}{r^*}+k_w^*w^*-k_p^*\left(\frac{\partial^2 w^*}{\partial r^{*2}}+\frac{1}{r^*}\frac{\partial w^*}{\partial r^*}\right)\Big|_{z=\frac{h}{2}}=0 \tag{45}$$

5. NUMERICAL RESULTS AND DISCUSSIONS

To investigate the convergence of the SAPM results for different grid sizes, an orthotropic annular/circular plate with the following properties is considered for various boundary conditions. The results are reported in Table 1. The nonzero components of the stiffness matrix are as follows [44]:

$$\begin{aligned}&C_{11}=1.078TPa;C_{22}=1.030TPa;C_{33}=32.6GPa;C_{12}=135GPa;C_{13}=15GPa;C_{23}=15GPa;\\&C_{44}=G_{rz}=319GPa;G_{\theta z}=394GPa;G_{r\theta}=157GPa;h=0.34nm;r_i/r_o=0.2;q=0.1GPa\end{aligned} \tag{46}$$

Table 1.
Convergence checking of dimensionless deflections of an orthotropic annular/circular plate versus the number of grid points.

n (number of domain nodes)	w^* Boundary Condition Type							
	C - C	S - S	C - S	S - C	C - F	F - C	S - F	F - S
3	0.000841	0.000841	0.000841	0.000841	-	0.01970	-	0.0839
5	0.003033	0.010096	0.006110	0.004381	-	0.04427	-	0.3823
7	0.003178	0.009951	0.005887	0.004519	0.02539	0.03438	0.3002	0.2077
9	0.003252	0.009828	0.005843	0.004549	0.04008	0.03242	0.1844	0.1847
11	0.003303	0.009801	0.005894	0.004574	0.04500	0.03198	0.1587	0.1795
13	0.003338	0.009820	0.005969	0.004597	0.04563	0.03180	0.1472	0.1782

Convergence is achieved with 11 grid points in the radial direction. For all cases, the number of grid points in the z direction is set to 5.

As the first step of validation, the deflection of an isotropic circular plate with the following properties and clamped edges is compared with results from Refs. [21, 45–47], as shown in Table 2:

$$E_r = E_\theta = E_z = 2MPa; \upsilon_{ij} = 0.3; h/r_o = 0.1 \quad (47)$$

Table 2.
Comparison of the non-dimensional deflection of an isotropic circular plate with clamped edges.

q*	$w^* = \frac{w}{r_o} = \frac{12q(1-\upsilon^2)r_o^3}{64Eh^3}$				
	[21]	[45]	[46]	[47]	Present study
0.0001	0.1685	0.1678	0.1687	0.1706	0.1774
0.0003	0.4642	0.4583	0.4655	0.5119	0.5322
0.001	1.0557	1.0509	1.0937	1.7069	1.7742

Good agreement is observed between the results, particularly with Ref. [47]. Additionally, the results for an isotropic annular plate with both clamped and simply supported edges are compared with those from Refs. [21, 48, 49] under the following conditions, as shown in Table 3:

$$E_r = E_\theta = E_z = 280GPa; \upsilon_{ij} = 0.288; h/r_o = 0.15; q^* = 0.054 \quad (48)$$

Table 3.
Comparison of the non-dimensional deflection of an isotropic annular plate with clamped and simply supported edges.

Study	w^*	
	Clamped	Simply supported
[21]	2.810	10.633
[48]	2.781	10.623
[49]	2.774	10.572
Present study	3.015	11.406

good agreement is observed.

To verify the results for orthotropic material behavior, and since deflection data for all boundary conditions considered in this study are not reported in the literature for an orthotropic annular/circular plate, the results are compared with those from a finite element model produced using ABAQUS software. The comparison, shown in Table 4, is based on the mechanical properties reported in Eq. (53), and the results demonstrate good agreement.

Table 4.
Comparison of the deflections for an orthotropic annular/circular plate with ABAQUS model for all boundary conditions.

Boundary condition type	w^*	
	ABAQUS model	Present study
C - C	0.00370	0.00330
S - S	0.01048	0.00980
C - S	0.00686	0.00589
S - C	0.00470	0.00457
C - F	0.04500	0.04500
F - C	0.03392	0.03198
S - F	0.14100	0.15870
F - S	0.18302	0.17950

To validate the deflection of an orthotropic annular/circular plate with elastic foundations, the results for the following properties are compared with those from Ref. [21], as shown in Table 5:

$$E_r = 1.06TPa;\ E_\theta = 0.85TPa;\ E_z = 32.6GPa;\ \upsilon_{ij} = 0.3;\ G_{rz}\,319GPa;\ h = 0.34nm;\ r_i / r_o = 0.2;$$
$$q = 0.1GPa;\ k_w = 1.13GPa/nm;\ k_p = 1.13GPa \cdot nm \tag{49}$$

Table 5.
Comparison of the dimensionless deflections with the literatures.

Boundary condition type	w^*		
	Ref. [21]		Present study (3D Elasticity)
	CPT	FSDT	
C – C	0.0030	0.0034	0.0031
S – S	-	0.0085	0.0085
C – S	-	0.0065	0.0053
F – C	-	0.026	0.0263

It is observed that the results show good agreement.

To verify the accuracy of the employed re-modified couple stress theory and the effect of scale parameters, the nonlinear bending analysis of both circular and annular micro/nanoplates under the following conditions is compared with the results reported by Reddy et al. [41], as shown in Table 6:

$$E_r = E_\theta = E_z = 1MPa;\upsilon_{ij} = 0.25;r_o = 1nm;h = 0.1nm \tag{50}$$

Table 6.
Comparison of the deflections for circular and annular micro/nanoplates with the literatures.

Study	w^*									
	Circular plate ($r_i = 0$)				Annular plate ($r_i = 0.25nm$)					
	F - C q = 100 Pa		F - S q = 100 Pa		F - C q = 100 Pa		C - F q = 50 Pa		F - S q = 50 Pa	
	$l/h=0$	$l/h=0.6$	$l/h=0$	$l/h=0.6$	$l/h=0$	$l/h=0.6$	$l/h=0$	$l/h=0.6$	$l/h=0$	$l/h=0.6$
[41] CPT	0.01757	0.0071	0.050	0.048	0.01624	0.0055	0.02358	0.01663	0.04273	0.02963
[41] FSDT	0.01829	0.0072	0.050	0.048	0.01685	0.0055	0.02358	0.01663	-	-
Present study	0.01822	0.0076	0.072	0.052	0.01761	0.0053	0.01860	0.01381	0.04407	0.02557

In all three parts of the validation, the results fall within an accurate range. Additionally, it is observed that, in most cases, the 3D elasticity theory estimates higher deflections compared to other theories such as CPT, FSDT, and TSDT.

To investigate the influence of MLSP, its effect was examined using different combinations of MLSP values for a plate with conditions based on Eq. (46). The results are reported in Table 7.It is observed that for CC, SS, CS, and SC boundaries, the use of MLSP decreases the deflection, indicating that the plates become stiffer. This observation aligns with the results reported by Reddy et al. [41]. The minimum deflection is occurs in $l_r/h=0$ and $l_\theta/h=1$ .with one exception: when $l_r/h=1$ and $l_\theta/h=0$,the deflection of the plates increases, indicating that the plates become more flexible. This behavior was not reported by [41], which could be due to the use of the isotropic form of modified couple stress theory in Ref. [41].

Table 7.
The influence of MLSP on the non-dimensional deflection of an orthotropic annular/circular micro/nanoplate for different B.C.s.

B.C.	w^*								
	$l_r/h=0$			$l_r/h=0.5$			$l_r/h=1$		
	$l_\theta/h=0$	$l_\theta/h=0.5$	$l_\theta/h=1$	$l_\theta/h=0$	$l_\theta/h=0.5$	$l_\theta/h=1$	$l_\theta/h=0$	$l_\theta/h=0.5$	$l_\theta/h=1$
C – C	0.00325	0.00312	0.00278	0.00325	0.00313	0.00278	0.00327	0.00314	0.00279
S – S	0.00983	0.00959	0.00890	0.00988	0.00964	0.00895	0.01006	0.00982	0.00909
C – S	0.00584	0.00553	0.00474	0.00585	0.00554	0.00475	0.00589	0.00558	0.00478
S – C	0.00455	0.00441	0.00403	0.00457	0.00443	0.00404	0.00463	0.00449	0.00410
C – F	0.04008	0.0412	0.0413	0.0404	0.0415	0.0417	0.0415	0.0427	0.0430
F – C	0.0324	0.0326	0.0362	0.0326	0.0328	0.0369	0.0331	0.0336	0.0395
S – F	0.1844	0.2027	0.2953	0.1866	0.2056	0.3038	0.1933	0.2174	0.3324
F – S	0.1847	0.1877	0.2299	0.1870	0.1909	0.2439	0.1944	0.2016	0.3045

Additionally, for FS, SF, CF, and FC boundaries, an increasing trend in deflection is observed, with the maximum occurring in $l_r / h = 1 \text{ and } l_\theta / h = 1$. The results indicate that the effect of MLSP also depends on the boundary conditions. Some literature [18-23] reports a reduction in deflection for these cases using nonlocal theories. Moreover, Reddy et al. [41] observed a reduction in deflection for FC, FS, and CF boundaries using modified couple stress theory.

It should be noted that the results obtained in the current study, as shown in Table 6, are consistent with those of [41] and indicate a reduction in plate deflection. This suggests that other parameters might influence the effect of MLSP. To further illustrate this point, additional examinations were conducted. A comparison between the results of the current study and the literature suggests that parameters such as the mechanical properties of the plates, aspect ratio, or thickness may affect the outcomes.

To investigate the influence of material behavior, the nonlinear bending of plates with the same dimensions as specified in Eq. (50) was examined for both the circular case (with ri=0) and the annular case (with ri=0.25 nm), using the mechanical properties defined in Eq. (46) (see Table 8).For plates with simply supported edges, both circular and annular, a reduction in deflection is observed. However, for clamped boundaries (C-F or F-C), an increase in deflection occurs. Thus, it can be concluded that the effect of MLSP depends on the material behavior.

Table 8.
The influence of MLSP on the non-dimensional deflection of circular and annular plates for various B.C.s.

Annular/Circular plate	B.C.	w^*	
		$l_r / h = l_\theta / h = 0$	$l_r / h = l_\theta / h = 0.6$
Circular	C	1.8061×10^{-8}	2.3300×10^{-8}
Circular	S	8.2966×10^{-8}	6.7321×10^{-8}
Annular	F-C	1.3939×10^{-8}	6.7850×10^{-8}
Annular	F-S	9.6360×10^{-8}	5.6600×10^{-7}
Annular	C-F	1.5044×10^{-8}	4.0009×10^{-8}

Next, to investigate the influence of aspect ratio and thickness, the nonlinear bending of plates was examined under the conditions specified in Eq. (46) for two different aspect ratios (thick and thin plates) (see Table 9). The results indicate that the bending behavior of thick and thin plates under the same conditions differs. Specifically, the decreasing effect of MLSP observed for thick plates with S-S, C-S, and S-C boundaries changes to an increasing effect as the plate becomes thinner.

Table 9.
The influence of aspect ratio on the non-dimensional deflection of annular/circular micro/nanoplate.

B.C.	w^*			
	$r_o = 2.5nm$		$r_o = 20nm$	
	$l_r / h = l_\theta / h = 0$	$l_r / h = l_\theta / h = 1$	$l_r / h = l_\theta / h = 0$	$l_r / h = l_\theta / h = 1$
C - C	0.003178	0.002727	21.474	20.084
S - S	0.009951	0.009026	65.394	66.893
C - S	0.005887	0.004791	54.294	56.701
S - C	0.004519	0.004041	33.604	34.040

Upon reviewing the literature, it is noted that some studies based on couple stress theory [41, 52, 53], nonlocal theory [19, 50, 51], or nonlocal strain gradient theory [54] report a decreasing effect on plate or beam deflection with an increase in the MLSP in couple stress theory or the nonlocal parameter in nonlocal theory. Conversely, other studies [53-57] observe an increasing effect. Additionally, Ref. [53] found that considering the nonlocal size effect results in greater deflection for the nonlinear bending of a micro/nanobeam, while accounting for strain gradient size dependency leads to the opposite observation.

Next, the effects of elastic foundation and temperature on deflection and thickness are investigated. From Table 7,it is deduced that C-C, S-S, C-S and S-C boundaries experiences their minimum deflection at $l_r / h = 0$, $l_\theta / h = 0$ and their maximum at $l_r / h = 1$, $l_\theta / h = 1$. Additionally, C-F, F-C, S-F and F-S boundaries show their minimum deflection at $l_r / h = 0$, $l_\theta / h = 1$ and their maximum deflection at $l_r / h = 1$, $l_\theta / h = 0$. Therefore, the influence of elastic foundations and thermal effects is examined for these specific cases for a plate with conditions specified in Eq. (46) with $\alpha = 2.02 \times 10^{-6}$ and $k_w = 1 GPa / nm$, $k_p = 1 GPa \cdot nm$, under thermal loading of $\Delta T = 500 C^\circ$ .Table 10 presents the effect of elastic foundations under mechanical loading, Table 11 shows the effect of a combination of thermo-mechanical loading, and Table 12 illustrates the influence of thermo-mechanical loading in the presence of elastic foundations.

Table 10.
The effect of elastic foundation on the non-dimensional deflection of annular/circular micro/nanoplate under mechanical loading.

B.C.	$l_r / h = l_\theta / h = 0$		$l_r / h = l_\theta / h = 1$		$l_r / h = l_\theta / h = 0$		$l_r / h = l_\theta / h = 1$	
	w^*	Δh^*	w^*	Δh^*	w^*	Δh^*	w^*	Δh^*
C – C	0.00311	0.0011	0.00268	0.0011	0.00313	0.0011	0.00269	0.001
S – S	0.00865	0.0012	0.00795	0.0012	0.00883	0.0012	0.0081	0.0012
C – S	0.00536	0.0012	0.00443	0.0012	0.00541	0.0012	0.00446	0.0012
S – C	0.00428	0.0011	0.00382	0.0011	0.00435	0.0011	0.00388	0.0011
C – F	0.03218	0.0011	0.0337	0.0016	0.03318	0.0011	0.03493	0.0016
F – C	0.02696	0.0013	0.02964	0.0018	0.02752	0.0013	0.03199	0.0019
S – F	0.1134	0.0015	0.1545	0.0018	0.1166	0.0015	0.1646	0.0018
F – S	0.08852	0.0018	0.09803	0.0022	0.09105	0.0018	0.1109	0.0023

Table 11.
The effect of thermo-mechanical loading on the non-dimensional deflection of annular/circular micro/nanoplate.

B.C.	$l_r / h = l_\theta / h = 0$		$l_r / h = l_\theta / h = 1$		$l_r / h = l_\theta / h = 0$		$l_r / h = l_\theta / h = 1$	
	w^*	Δh^*	w^*	Δh^*	w^*	Δh^*	w^*	Δh^*
C – C	0.00355	0.0038	0.00299	0.0038	0.00358	0.0038	0.0031	0.0038
S – S	0.01361	0.0026	0.01187	0.0028	0.0140	0.0026	0.0122	0.0026
C – S	0.00722	0.0026	0.00562	0.0026	0.00730	0.0026	0.0056	0.0026
S – C	0.00509	0.0037	0.00446	0.0037	0.00520	0.0037	0.00454	0.0037
C – F	0.0404	0.0038	0.0472	0.0038	0.0418	0.0025	0.0494	0.0038
F – C	0.0398	0.0037	0.0478	0.0058	0.0409	0.0037	0.0544	0.0059
S – F	0.1425	0.0025	0.2978	0.0031	0.1472	0.0025	0.3279	0.0031

Table 12.
The influence of thermo-mechanical loading on the non-dimensional deflection of annular/circular micro/nanoplate rested on elastic foundation.

B.C.	$l_r/h=l_\theta/h=0$		$l_r/h=l_\theta/h=1$		$l_r/h=l_\theta/h=0$		$l_r/h=l_\theta/h=1$	
	w^*	Δh^*	w^*	Δh^*	w^*	Δh^*	w^*	Δh^*
C – C	0.0034	0.0039	0.00293	0.0039	0.00346	0.0039	0.0029	0.0039
S – S	0.01149	0.0027	0.01030	0.0027	0.0118	0.0027	0.0105	0.0027
C – S	0.00653	0.0027	0.00522	0.0027	0.0066	0.0027	0.00526	0.0027
S – C	0.00482	0.0038	0.00428	0.0038	0.0049	0.0038	0.00435	0.0038
C – F	0.0326	0.0026	0.0367	0.0038	0.0336	0.0026	0.03814	0.0038
F – C	0.0322	0.0040	0.0373	0.0060	0.0330	0.0040	0.0414	0.0062
S – F	0.1005	0.0027	0.01702	0.0036	0.1029	0.0027	0.1806	0.0036
F – S	0.2184	0.0042	0.3079	0.0057	0.2313	0.0043	0.4722	0.0072

It is observed that employing an elastic foundation and increasing temperature do not cause significant changes in the effect of MLSP or the behavior of plate deflection. As expected, the use of an elastic foundation reduces the plate deflection, while an increase in temperature leads to greater deflection. The most significant increase in deflection due to thermal loading is observed under S-S boundary conditions, while the minimum increase occurs under C-F boundary conditions. Conversely, the most significant decrease in deflection due to the elastic foundation is observed under F-S and S-F boundary conditions, with the minimum decrease occurring under C-C boundary conditions.

The most significant thickness variation under mechanical loading and in the absence of an elastic foundation is observed for F-S and S-F conditions, where increasing MLSP has a notable effect on the plate thickness, especially for plates with one free edge. The inclusion of an elastic foundation does not show a considerable impact on plate thickness under mechanical loading. However, with thermo-mechanical loading, significant changes in plate thickness are observed, particularly in plates with no free edges. When an elastic foundation is added under thermo-mechanical loading, thickness variation becomes more pronounced for plates with one free edge, especially under the F-C boundary condition.

The effect of thickness variation on an annular plate with conditions of $l_r/h=1, l_\theta/h=1$, and different boundary conditions, without an elastic foundation, is investigated and presented in Fig. 3. The plate properties are based on Eq. (46). It is observed that as the thickness increases, the deflection decreases, with the most noticeable reduction occurring in the S-S case. Additionally, it is noted that the effect of boundary conditions diminishes with increasing thickness.

The influence of temperature variation on deflection and thickness for the conditions specified in Eq. (46) and $l_r/h=1, l_\theta/h=1$, with different boundary conditions and in the absence of an elastic foundation, is examined. The results are reported in Fig. 4 and Fig. 5, respectively. It is observed that increasing the temperature leads to increased deflection, with the most significant effect occurring in the S-S boundary condition which can be due to the most available degree of freedom in S condition. Additionally, temperature increases result in linear variation of thickness, which is more pronounced in C-C and S-C (plates with an outer clamped edge) compared to S-S and C-S boundaries which this linear variations shows direct effect between temperature and thickness variation.

As the final step, the influence of elastic foundation parameters on deflection is investigated. The variation of plate deflection under the conditions specified in Eq. (46) versus changes in elastic foundation parameters for different boundaries and $l_r/h=1, l_\theta/h=1$ is reported in Fig. 6 and Fig. 7. The results indicate that the effect of the Winkler parameter on decreasing deflection is much more pronounced compared to the Pasternak parameter. Nonlinear behavior is observed with the Winkler foundation, while linear behavior is noted with increasing stiffness coefficients of the Pasternak elastic foundation.

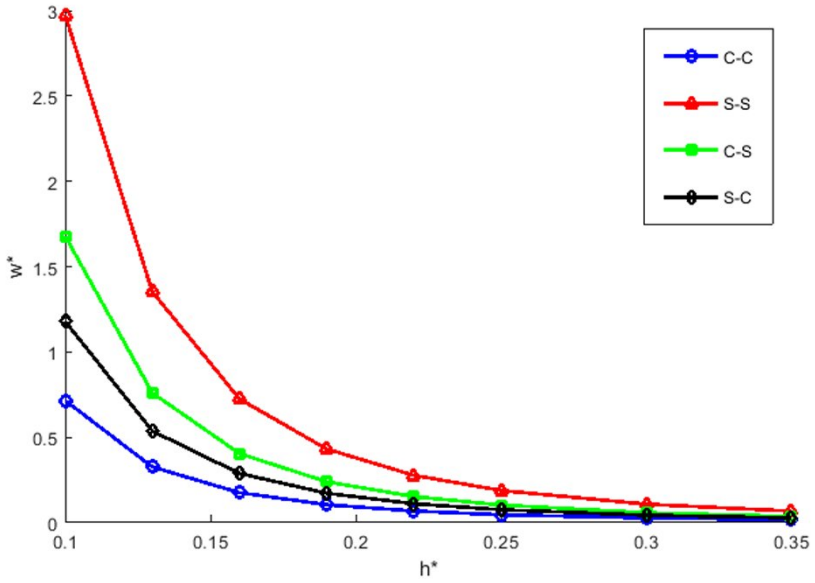

Fig. 3
The variation of non-dimensional deflection versus thickness of annular micro/nanoplate.

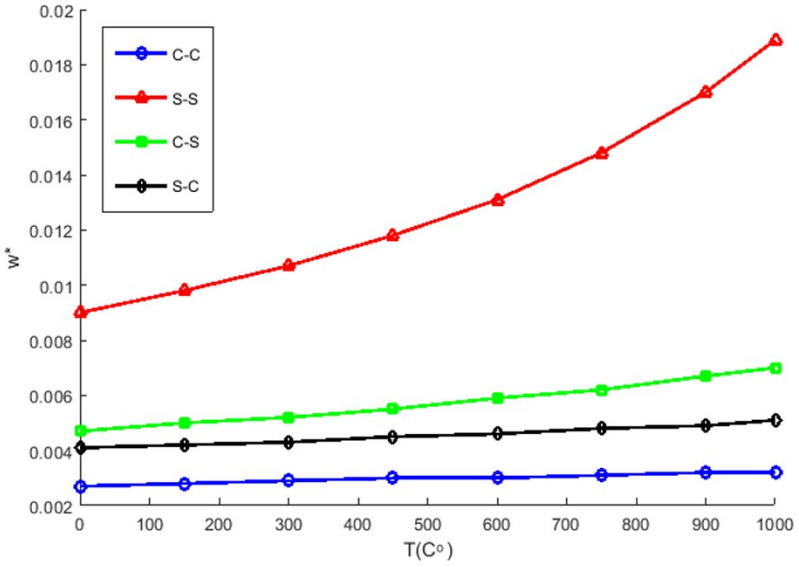

Fig. 4
The variation of non-dimensional deflection versus temperature variation of annular micro/nanoplate.

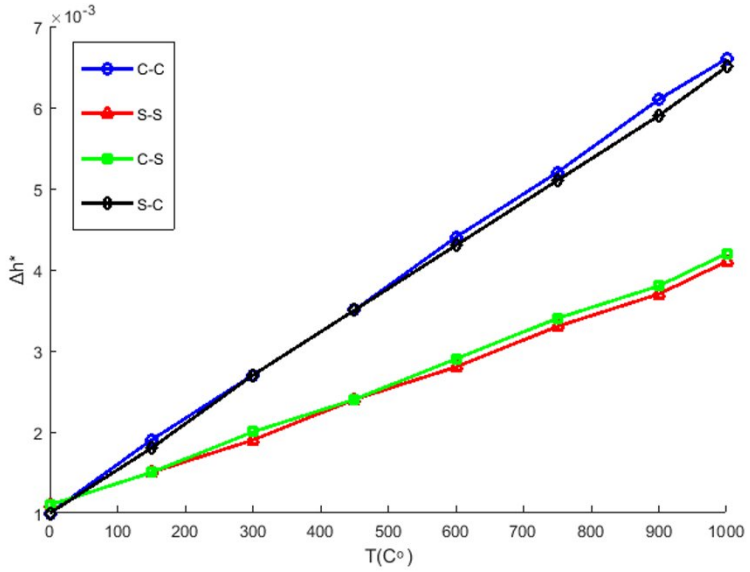

Fig. 5
The variation of non-dimensional thickness versus temperature variation of annular micro/nanoplate.

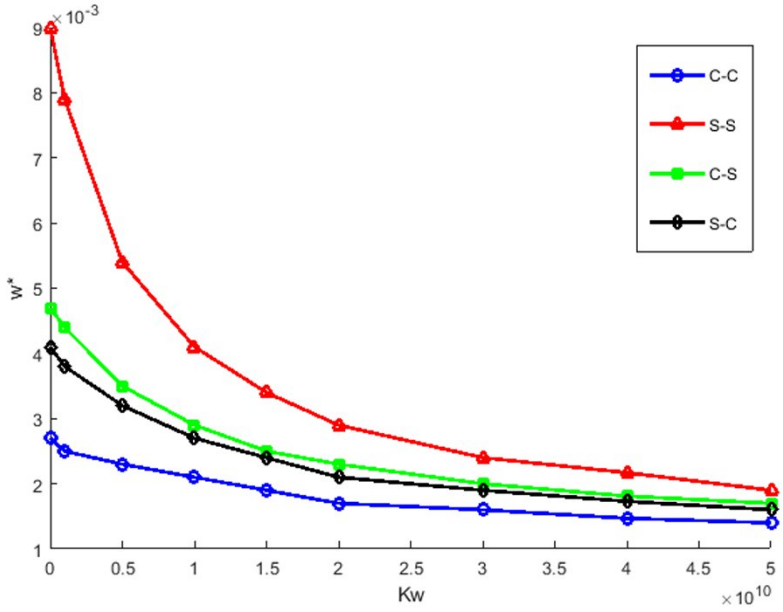

Fig. 6
The variation of non-dimensional deflection versus Winkler elastic foundation of annular micro/nanoplate.

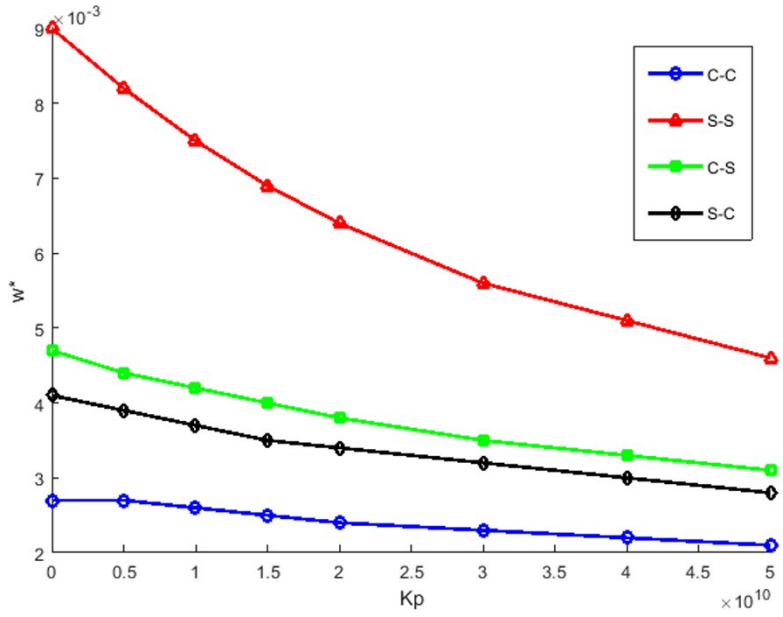

Fig. 7
The variation of non-dimensional deflection versus Pasternak elastic foundation of annular micro/nanoplate.

6. CONCLUSION

In this study, a new numerical solution approach based on 3D elasticity theory and the SAPM is presented for the nonlinear thermo-mechanical bending analysis of orthotropic annular/circular micro/nanoplates resting on an elastic foundation, using re-modified couple stress theory. The effects of various parameters, including boundary conditions, couple stress scale parameters, aspect ratio, thickness, thermal stresses, and elastic foundation parameters, are investigated. Some of the key results are summarized below:

- The results obtained using 3D elasticity theory are higher compared to those obtained with CPT, FSDT, and TSDT under the same conditions.
- The influence of MLSP for isotropic materials with a single MLSP may differ from the effect of various combinations of MLSPs for anisotropic materials with three MLSPs.
- The influence of MLSPs may vary depending on the boundary conditions and different mechanical properties.
- Changing the plate aspect ratios, especially by making the plate thicker or thinner, can alter the effect of MLSPs.
- The influence of MLSP does not show significant changes when an elastic foundation is added or thermal loading is applied.
- The extent of the decreasing effect of the elastic foundation and the increasing effect of thermal loading on deflection depends on the boundary conditions.
- The most significant variation in plate thickness occurs in plates with one free edge, with thickness increasing under thermal loading.
- The effect of thermal loading on plate thickness is more pronounced in plates without free edges.
- Increasing the thickness decreases deflection, with the effect being more pronounced for the S-S boundary condition.
- The increasing effect of temperature on deflection is more significant for S-S boundaries.
- The influence of temperature on thickness variation increases linearly and is more pronounced in plates with an outer clamped edge.
- The decreasing effect of the Winkler parameter on deflection is more pronounced than that of the Pasternak parameter.

FUNDING STATEMENT

This research did not receive any specific grant from funding agencies in the public, commercial, or not-for-profit sectors.

CONFLICT OF INTEREST

The author declares that there is no conflict of interest regarding the publication of this article.

REFERENCES

[1] Rafiee M.A., Rafiee J., 2009, Enhanced mechanical properties of nano composites at low graphene contents, ACS Nano3: 3884-90.
[2] Golkarian A.R., Jabbarzadeh M., 2012, The Attitude of Variation of Elastic Modules in Single Wall Carbon Nanotubes: Nonlinear Mass-Spring Model, J of Solid Mech 4: 106-113.
[3] Golkarian A,R., Jabbarzadeh M., 2013, The density effect of van der Waals forces on the elastic modules in graphite layers, Comput Mater Sci 74: 138-142.
[4] Shariati A.A., Golkarian A.R., Jabbarzadeh M., 2014, Investigation of Vibrational Behavior of Perfect and Defective Carbon Nanotubes Using Non–Linear Mass–Spring Model, J of Solid Mech 6: 255-264.
[5] Golkarian A.R., Jabbarzadeh M., 2015, The influence of interlayer interactions on the mechanical properties of polymeric nanocomposites, JSCS–4810 80(11): 1449-1459.
[6] Bao W.X., Zhu C.C., 2004, Simulation of young's modulus of single-walled carbon nanotubes by molecular dynamics, Physica B 352: 156-63.
[7]Zhao H., Min K., 2009, Size and chirality dependent elastic properties of graphene nanoribbons under uniaxial tension, Nano Letter 9: 3012-15.
[8] Toupin R.A., 1962, Elastic materials with couple stresses, Arch Ration Mech Anal 11: 385-414.
[9] Mindlin R.D., Tiersten H.F., 1962, Effects of couple-stresses in linear elasticity, Arch Ration Mech Anal 11: 415-448.
[10] Mindlin R.D., 1963, Influence of couple-stresses on stress concentrations, Exp Mech 3: 1-7.
[11] Koiter W.T., 1964, Couple-stresses in the theory of elasticity: I and II. Proc K Ned Akad Wet B 67: 17-44.
[12] Aifantis E.C., 1999, Strain gradient interpretation of size effects, Int J Fract. 95: 1-4.
[13] Eringen A.C., 1972, Nonlocal polar elastic continua, Int J Eng Sci 10: 1-16.
[14] Gurtin M.E., Weissmuller J., Larche F., 1998, The general theory of curved deformable interfaces in solids at equilibrium, Philos Mag A: 1093-1109.
[15] Yang F., Chong A.C.M., Lam D.C.C., Tong P., 2002, Couple stress based strain gradient theory for elasticity, Int J Solids Struct 39: 2731-43.
[16] Reddy J.N., Berry J., 2012, Nonlinear theories of axisymmetric bending of functionally graded circular plates with modified couple stress, Compos Struct 94 (12): 3664-68.
[17] Reddy J.N., Kim J., 2012, A nonlinear modified couple stress-based third-order theory of functionally graded plates, Compos Struct 94: 1128-1143.
[18] Dastjerdi S., Jabbarzadeh M., 2016, Nonlinear bending analysis of bilayer orthotropic graphene sheets resting on Winkler-Pasternak elastic foundation based on Nonlocal Continuum Mechanics, Compos Part B 87: 161-175.
[19] Dastjerdi S., Jabbarzadeh M., Aliabadi S., 2016, Nonlinear static analysis of single layer annular/circular graphene sheets embedded in Winkler–Pasternak elastic matrix based on non-local theory of Eringen, Ain Shams Eng J 7: 873-884.
[20] Dastjerdi S., Lotfi M., Jabbarzadeh M., 2016, The effect of vacant defect on bending analysis of graphene sheets based on the Mindlin nonlocal elasticity theory, Compos Part B 98: 78-87.
[21] Dastjerdi S., Jabbarzadeh M., 2017, Non-linear bending analysis of multi-layer orthotropic annular/circular graphene sheets embedded in elastic matrix in thermal environment based on non-local elasticity theory, App Math Model 41: 83-101.
[22] Dastjerdi S., Jabbarzadeh M., 2016, Nonlocal Bending Analysis of Bilayer Annular/Circular Nano Plates Based on First Order Shear Deformation Theory, J of Solid Mech 8: 645-661.
[23] Dastjerdi S., Jabbarzadeh M., 2016, Non-Local Thermo-Elastic Buckling Analysis of Multi- Layer Annular/Circular Nano-Plates Based on First and Third Order Shear Deformation Theories Using DQ Method, J of Solid Mech 8: 859-874.
[24] Thai H.T., Choi D.H., 2013, Size-dependent functionally graded Kirchhoff and Midline plate models based on a modified couple stress theory, Compos Struct 95: 142-153.

[25] Thai H.T., Kim Se., 2013, A size-dependent functionally graded Reddy plate model based on a modified couple stress theory, Compos Part B 50: 1636-1645.
[26] Thai H.T., Vo T.P., 2013, A size-dependent functionally graded sinusoidal plate model based on a modified couple stress theory, Compos Struct 96: 376-383.
[27] Sahmani S., Ansari R., 2013, On the free vibration response of functionally graded higher-order shear deformable microplates based on the strain gradient elasticity theory, Compos Struct 95: 430-442.
[28] Daneshmehr A., Rajabpoor A., pourdavood M., 2014, Stability of size dependent functionally graded nanoplate based on nonlocal elasticity and higher order plate theories and different boundary conditions, Int J Eng Sci 82: 84-100.
[29] Ghorbanpour-Arani A.H., Abdollahian M., Ghorbanpour Arani A., 2020, Nonlinear dynamic analysis of temperature-dependent functionally graded magnetostrictive sandwich nanobeams using different beam theories, Journal of the Brazilian Society of Mechanical Sciences and Engineering 42: 314.
[30] Ghorbanpour Arani A., Jamali M., Ghorbanpour-AraniA.H., Kolahchi R., MosayyebiM., 2016, Electro-magneto wave propagation analysis of viscoelastic sandwich nanoplates considering surface effects, Proceeding of the institution of Mechanical Engineers, Part C: Journal of Mechanical Engineering Science 231: 2.
[31] Ghorbanpour-Arani A.H., RastgooA., Sharafi M.M., Kolahchi R., Ghorbanpour Arani A., 2016, Nonlocal viscoelasticity based vibration of double viscoelastic piezoelectric nanobeam systems, Meccanica 51: 25-40.
[32] Ghorbanpour Arani A., Haghparast E., Ghorbanpour Arani A.H., 2014, Size-dependent vibration of double-bonded carbon nanotube-reinforced composite microtubes conveying fluid under longitudinal magnetic field, polymer composites 37: 5, 1375-1383.
[33] Ghorbanpour-Arani A.H., Rastgoo A., Hafizi Bidgoli A., Kolahchi R., Ghorbanpour Arani A., 2017, Wave propagation of coupled double-DWBNNTs conveying fluid-systems using different nonlocal surface piezoelasticity theories, Mechanics of Advanced Materials and Structures 24: 14.
[34] Haghparast E., Ghorbanpour-Arani A.A., Ghorbanpour Arani A., 2020, Effect of Fluid–Structure Interaction on Vibration of Moving Sandwich Plate With Balsa Wood Core and Nanocomposite Face Sheets, International Journal of Applied Mechanics 12: 07 2050078.
[35] Ghorbanpour-Arani A.A., Khoddami Maraghi Z., Ghorbanpour Arani A., 2023, The Frequency Response of Intelligent Composite Sandwich Plate Under Biaxial In-Plane Forces, Journal of Solid Mechanics 15: 1 1-18.
[36] Kashtalyan M., 2004, Three-dimensional elasticity solution for bending of functionally graded rectangular plates, Eur J MechA Solids 23: 853-864.
[37] Kashtalyan M., Menshykova M., 2009, Effect of a functionally graded interlayer on three-dimensional elastic deformation of coated plates subjected to transverse loading, Compos Struct 89: 167-176.
[38] Huang Z.Y., Lu C.F., Chen W.Q., 2008, Benchmark solutions for functionally graded thick plates resting on Winkler–Pasternak elastic foundations, Compos Struct 85: 95-104.
[39] Woodward B., Menshykova M., 2011, Three-dimensional elasticity solution for bending of transversely isotropic functionally graded plates, Eur J Mech A Solids 30: 705-718.
[40] Salehipour H., Nahvi H., Shahidi A., Mirdamadi H.R., 2017, 3D elasticity analytical solution for bending of FG micro/nanoplates resting on elastic foundation using modified couple stress theory, App Math Model 47: 174-188.
[41] Reddy J.N., Romanoff J., Loya J.A., 2016, Nonlinear finite element analysis of functionally graded circular plates with modified couple stress theory, Euro J of Mech A/Solids 56: 92-104.
[42] Yang F., Chong A.C.M., Lam D.C.C., Tong P., 2002, Couple stress based strain gradient theory for elasticity, Int J Solids Struct 39: 2731-43.
[43] Chen W., Li X., 2014, A new modified couple stress theory for anisotropic elasticity and microscale laminated Kirchhoff plate model, Arch Appl Mech 84 (3): 323-41.
[44]Hosseini Kordkheili S.A., Moshrefzadeh-Sani H., 2013, Mechanical properties of double-layered graphene sheets, Comput Mat Sci 69: 335-343.
[45] Altekin M., Yu¨ kseler R.F., 2011, London, U.K. WCE. In: Proof the World Cong on Eng.
[46] Timoshenko S., Woinowsky-Krieger S., 1959, Theories of Plates and Shells. New York: McGraw-Book Company, p. 410-412.
[47] Szilard R., 1974, Theory and Analysis of Plates, Englewood Cliffs: Prentice-Hall Inc. p. 622.
[48] Reddy J.N., Wang C.M., Kitipornchai S., 1999, Axisymmetric bending of functionally grade circular and annular plates, Euro J MechA/Solids18: 185-99.
[49] Golmakani M.E., 2013, Non-linear bending analysis of ring-stiffened functionally graded circular plates under mechanical and thermal loadings, Int J Mech Sci 79: 130-42.
[50] Sobhy M., 2014, Thermo mechanical bending and free vibration of single-layered graphene sheets embedded in an elastic medium, Physica E 56: 400-409.
[51] Panyatong M., Chinnaboon B., Chucheepsakul S., 2018, Nonlinear bending analysis of nonlocal nanoplates with general shapes and boundary conditions by the boundary-only method, Eng Anal with Bound Elem 87: 90-110.
[52] Kim J., Reddy J.N., 2013, Analytical solutions for bending, vibration, and buckling of FGM plates using a couple stress-based third-order theory, Compos Struct 103: 86-98
[53] Shaat M., Mahmoud F.F., Gao X.L., Faheem A.F., 2014, Size-dependent bending analysis of Kirchhoff nano-plates based on a modified couple-stress theory including surface effects, Int J of Mech Sci 79: 31-37.

[54] Sahmania S., Mohammadi Aghdama M., Rabczuk T., 2018, Nonlinear bending of functionally graded porous micro/nano-beams reinforced with graphene platelets based upon nonlocal strain gradient theory, Compos Struct 186: 68-78.
[55] Sobhy M., 2015, Levy-type solution for bending of single-layered graphene sheets in thermal environment using the two-variable plate theory. Int J of Mech Sci 90: 171-178.
[56] Yan J.W., Tong L.H., Li C., Zhu Y., Wang Z.W., 2015, Exact solutions of bending deflections for nano-beams and nano-plates based on nonlocal elasticity theory, Compos Struct 125: 304-313.
[57] Kolahchi R., 2017, A comparative study on the bending, vibration and buckling of viscoelastic sandwich nano-plates based on different nonlocal theories using DC, HDQ and DQ methods, Aero Sci & Tech 66: 235-248.